Distinct Magnetospheric Responses to Southward IMF in two Substorms

Mostafa El-Alaoui[1], M. Ashour-Abdalla[1], R. L. Richard[1],
L. A. Frank[2], W. R. Paterson[2], and J. B. Sigwarth[2]

[1]Institute of Geophysics and Planetary Physics, University of California Los Angeles
405 Hilgard Ave, Los Angeles, CA 90095-1567;
mostafa@igpp.ucla.edu

[2]Department of Physics and Astronomy, The University of Iowa

Abstract. Solar wind plasma parameters and the Interplanetary Magnetic Field (IMF) observed by the WIND spacecraft upstream of the bow shock were used as input to magnetohydrodynamic (MHD) simulations of two substorm events. The power deposited into the ionosphere due to electron precipitation was calculated both from VIS observations and from the simulations.

1. Introduction

Global MHD simulations have been used for more than 20 years to help understand the interaction of the solar wind with the Earth's magnetosphere [e.g. *Leboeuf et al.*, 1978; *Lyon et al.*, 1980]. Initially MHD models used idealized solar wind conditions (e.g. with IMF B_z constant and northward or southward) to identify the principal features of solar wind-magnetosphere coupling [e.g. *Ogino and Walker*, 1984]. Advances in computers and improved numerical techniques have allowed the construction of high-resolution three-dimensional models to study this interaction. More recently, observed solar wind plasma and magnetic field time series have been used to drive three-dimensional global MHD simulations. Results from these simulations have been directly compared to in situ spacecraft observations [e.g. *Frank et al.*, 1995]. Studies of quiet magnetospheric intervals were considered first [e.g. *Ashour-Abdalla et al.*, 1998] before studying the highly dynamic magnetotail during substorms [*Raeder et al.*, 1998; *Ashour-Abdalla et al.*, 1999; *El-Alaoui*, 2001]. Studies using the approach of using observed values as model input have successfully reproduced a great deal of the observed dynamics of the magnetosphere. These studies are best performed for intervals during which spacecraft are positioned close to regions where important dynamical events are occurring.

This paper is concerned with two substorm events that were first identified by *Frank et al.* [2001]. Two approaches have been taken in carrying out comparisons between simulation results and spacecraft observations. In the first synthetic auroral emissions are derived from the simulation results and compared with images from auroral spacecraft [*Fedder et al.*, 1995]. Because the aurora maps to a large region of the near-Earth magnetotail, this approach allows comparisons of multiple individual features.

In the second approach time series from the simulations are compared with those measured by spacecraft in the magnetotail. This second approach has been effective in studies of different regions in the magnetotail. Such studies have addressed the dynamics of the magnetospheric boundary [*Berchem et al.*, 1998] and the plasma sheet during substorm intervals [*Ashour-Abdalla et al.*, 1999]. In these studies, the simulation results and magnetotail observations showed general agreement in their description of the spacecraft motion through different regions, though many observed details were not reproduced by the simulations, particularly in regions with sharp gradients. In spite of its limitations MHD modeling is the only approach that can reproduce the effect of solar wind variations on the magnetosphere which then can be directly compared with satellite time series in specific cases.

2. Model

The global MHD simulation code solves the resistive MHD equations as an initial value problem for the magnetosphere and a potential equation for the ionosphere [*Raeder et al.,* 1998]. Since the use of a high-order hybrid scheme with increased spatial resolution minimizes the amount of numerical dissipation that occurs in the computation, we also include a resistive term in Ohm's law, $\mathbf{E} = -\mathbf{v} \times \mathbf{B} + \eta\mathbf{J}$; the resistivity η is a nonlinear function of the local current density j such that $\eta = \alpha j^2$, where α is an empirically determined parameter ($\alpha << 1$). To avoid spurious dissipation we include a threshold that is also a function of the local normalized current density; this threshold is calibrated such that explicit resistivity is switched on only at a few grid points in strong current sheets.

The solar wind magnetic field, density, temperature, and velocity are imposed on the sunward face of the simulation box; open boundary conditions ($\partial/\partial n = 0$) are assumed for all of the other sides of the box. The dimensions of the simulation box are 25 R_E in the sunward direction, 300 R_E along the tail and 50 R_E in each transverse direction. With such a large simulation domain, all flows at the external boundaries are in the super magnetosonic regime, which prevents any information from propagating back from the boundaries and affecting the physical processes occurring in the simulations. A large number of grid points ($2 \cdot 10^6$) are used, and equations are solved on a stretched Cartesian computational grid, which permits us to increase substantially the grid density in the plasma sheet region.

The MHD model has an inner spherical boundary with a radius of 3 R_E. This boundary is designed to exclude the region where the Alfvén velocity becomes too large to use a reasonable time step. Since this near-Earth region is dominated by the terrestrial field, this procedure does not significantly affect the simulation. Closure of FAC is ensured by solving self-consistently the ionospheric potential equation:

$$\nabla(\Sigma \cdot \nabla\Phi) = -j_{\parallel} \sin\theta,$$

where Φ denotes the ionospheric potential, Σ is the tensor of the ionospheric conductance, $j_{\parallel}$ is the FAC at the inner magnetospheric boundary mapped onto the polar cap, and θ is the inclination of the magnetic field at the ionosphere. The boundary condition $\Phi = 0$ is applied at the equator.

Our present model uses three ionization sources to compute the height-integrated ionospheric Hall and Pedersen conductivities. The first component is a result of solar EUV ionization and is evaluated by using the *Moen and Brekke* [1993] model. The second source is made up of precipitating electrons associated with upward FACs and is computed by using the relation established by *Lyons et al.* [1979]. The third contribution comes from diffuse electron precipitation and assumes a full loss cone at the inner boundary. The conductances are calculated from the precipitation parameters (mean energy and energy flux) by using the *Robinson et al.* [1987] empirical relation. The ionospheric potential is then mapped to the inner boundary where it is used as a boundary condition for the flow velocity $\mathbf{v} = -\nabla\Phi \times \mathbf{B}/B^2$. With our present MHD grid, the effective spatial resolution of the ionospheric parameters in the auroral zone is 0.5° in magnetic latitude and 3° in magnetic longitude. A detailed description of the MHD model can be found in *Raeder et al.,* [1998].

3. Event studies

Frank et al. [2001] conducted an investigation of 112 auroral substorm events observed by the Polar VIS instrument in 1996. They searched for events where the auroral onset region could be magnetically mapped to a location near Geotail and earthward of it. Two events were found that satisfied their criteria; one on July 2 and one on September 4. In this paper we describe global MHD simulations of these two substorm events. We focus on the results of calculations of the power deposited into the ionosphere and comparisons of this to observations.

1.1 July 1-2, 1996 event

On July 1-2, 1996, from about 1800 UT (July 1) to 0800 UT (July 2), the WIND spacecraft was located 211 R_E upstream of Earth in the dusk sector. Figure 1 shows WIND's measurements of the IMF and the solar wind plasma (solid lines) and the solar wind parameters at the upstream edge of the simulation box (dashed lines).

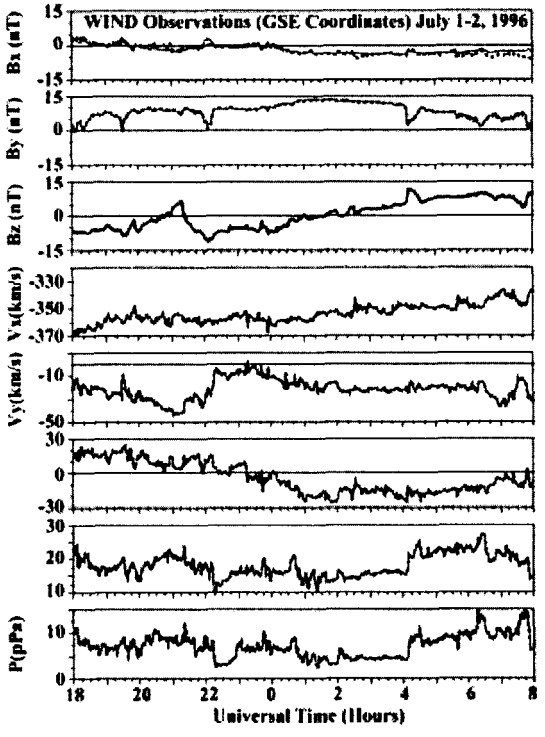

Figure 1. Solar wind parameters for July 1-2, 1996. The first three panels show WIND measurements of the magnetic field components, then the velocity components, proton density, and the last panel the thermal pressure. The dashed lines in the first three panels show the MHD simulation input using the technique described in section 2.2 of *El-Alaoui* [2001].

In order to keep the magnetic field divergence free during this event the method described in section 2.2 of *El-Alaoui* [2001] is used to model the three components of the field. This method, which is based on minimum variance, does a good job in reproducing the magnitude and variation of the IMF. During the whole time interval the IMF B_y component was strong and directed duskward with occasional decreases. The IMF B_x component was relatively weak and drifted from the sunward direction to anti-sunward. The B_z component was southward until 2100 UT (July 1, 1996) when it turned northward for about 15 minutes. It then turned southward again and remained southward until 0100 UT. The solar wind density was about 15 to 20 cm^{-3}, which is about 3 times the typical density of the solar wind. Meanwhile, the solar wind speed was slowly decreasing from about 370 km/s to about 340 km/s.

Figure 2 shows the total power deposited into the ionosphere from VIS observations (dashed line) and calculations from the MHD simulation of the power deposited into the ionosphere as a function of time (heavy line). The total power was calculated by integrating the expression below over a sphere at 1 R_E.

$$Power = \int_S \left(n_e k T_e \sqrt{\frac{k T_e}{2\pi m_e}} + J_{\parallel} \Delta\phi_{\parallel} \right) ds$$

In this expression n_e and T_e are the magnetospheric electron density and temperature and $J_{\parallel}$ is the parallel current and $\Delta\Phi_{\parallel}$ is the field-aligned potential drop [*Knight*, 1973]. Their values were calculated at the inner boundary of the simulation at 3 R_E and mapped along magnetic field lines to the ionosphere by using a dipole magnetic field to represent the internal field of the Earth.

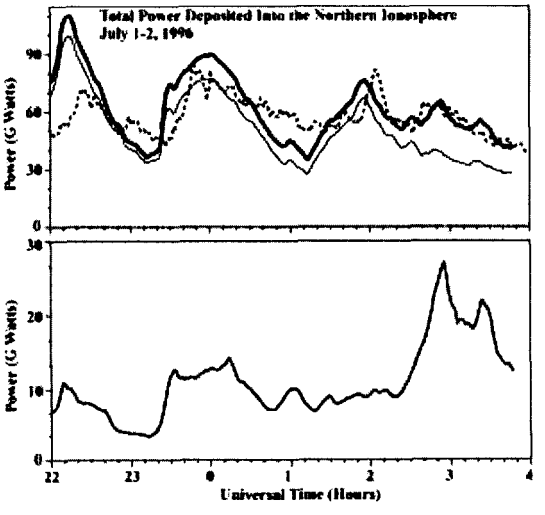

Figure 2. A comparison of time series from VIS observations and results from a global MHD simulation of the power deposited into the northern ionosphere. The second panel shows the power associated with upward Region 1 field aligned currents.

The first contribution to the power comes from diffuse electron precipitation [*Kennel and Petschek*, 1966]. The second source is precipitating electrons associated with upward FACs. We compute the mean energy $e\Delta\Phi_{\parallel}$ and the energy flux of precipitating electrons that are accelerated by the parallel potential drop $\Delta\Phi_{\parallel}$ [*Knight*, 1973; *Lyons et al.*, 1979].

The light line in the first panel of Figure 2 shows the contribution of the diffuse precipitation (the first term in the integral). The heavy curve shows the total power including both diffuse and discrete precipitation. The dashed line shows the observed power deposited into the ionosphere calculated from VIS observations. The second panel in the figure shows a plot of the power due to FACs (the second term in the integral). Only Region 1 currents are included in this calculation, since the MHD model does not fully resolve the Region 2 field-aligned currents.

During this event the simulations suggest that the discrete aurora typically contributes less than 15% of the power, although after 0230 UT it seemed that the discrete contribution approaches the diffuse contribution. Both observations and simulations suggest that the power deposited into the ionosphere showed large variation versus time.

During this whole time interval the minimum power deposited into the ionosphere was ~30 GW. The power increased to over 100 GW during the time of enhanced activity. *Spiro et al.* [1982] developed an empirical relationship between the *AE* index and the precipitated power that gives about 100 GW for major substorms. This is in good agreement with the simulation results.

Another feature of this interval was small scale oscillations in the solar wind dynamic pressure. We looked for a signature of these oscillations in the ionospheric parameters. The parameter that most closely followed the oscillations was the power deposited into the northern ionosphere due to the parallel plasma flow ($\int n_e k T_e V_{\|} ds$). This parameter may reflect ULF waves in the simulated magnetosphere. The solid black curves in both panels of Figure 3 show the parallel plasma flow. This power is only 0.1 to 0.3% of the total power deposited into the ionosphere. The dashed line in the first panel of Figure 3 shows the solar wind dynamic pressure shifted by 76 minutes to account for the solar wind propagation from WIND location; in the second panel the dashed line represent the IMF B_z component shifted by the same amount. It is interesting to note that each small-scale peak in the solar wind dynamic pressure evidently corresponds to a peak in the calculated power (Figure 3).

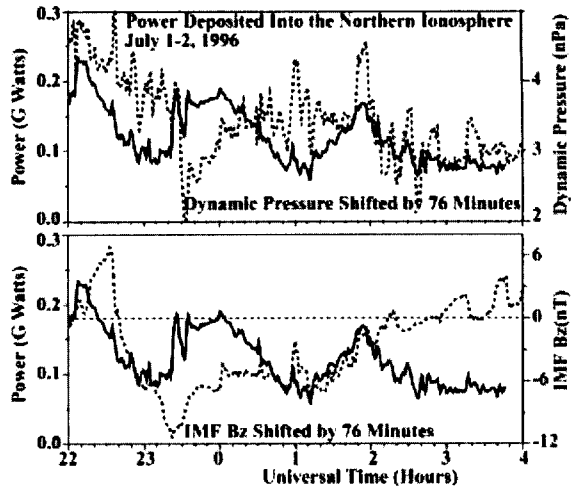

Figure 3. The solid black curves show the simulated power deposited into the northern hemisphere ionosphere due to the parallel plasma bulk flow. The dashed line show time shifted solar wind dynamic pressure (top) and IMF Bz (bottom) according to the scales on the right. 0200 UT is the time of substorm onset.

1.2 September 4, 1996

Solar wind plasma parameters and the IMF observed by the WIND spacecraft located at $x = 81$ R_E are shown in Figure 4. The IMF rapidly turned southward at 1956 UT and remained southward until ~2250 UT, when it turned northward. While it was southward it underwent several significant changes in magnitude; at around 2130 UT the IMF B_z decreased in magnitude to nearly zero and continued to fluctuate until about 2200 UT, when it increased in magnitude again. The IMF then changed from about -9 nT to -3 nT (at ~2230 UT) and to northward (at ~2250 UT) in a step wise fashion. The IMF B_y component was dawnward throughout most of the interval except for a brief excursion around 2050 UT. The B_x component showed behavior very similar to the IMF B_z component. The solar wind velocity was on average, 375 km/s throughout the interval. A high density of 13 cm^{-3} prevailed during the interval of southward IMF.

Figure 5 shows, in a similar format to Figure 2, the total power deposited into the northern hemisphere ionosphere by various components of the precipitation.

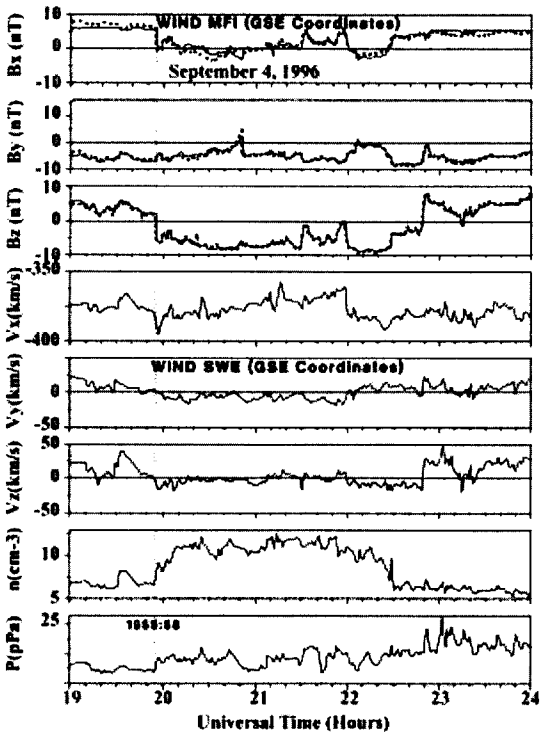

Figure 4. IMF and plasma parameters from the WIND spacecraft for September 4, 1996.

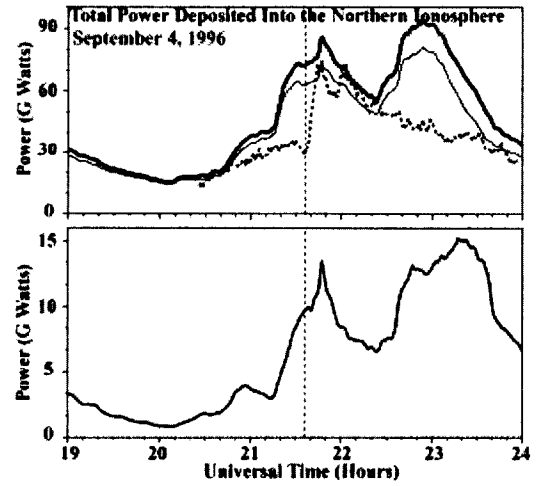

Figure 5. A comparison of time series from VIS observations (dashed line) and result from a global MHD simulation (solid lines).

The contribution of the diffuse precipitation (light line in top panel) and the total power including both diffuse and discrete precipitation (black curve in top panel) are shown. The dashed line shows the observed power deposited into the ionosphere calculated from VIS observations. Both show large variations in the power deposited into the ionosphere. However, the simulation and the observations have significant differences. The substorm onset in the MHD simulation preceded the observed onset by about 15 minutes; although the peak energies are comparable. This may be due to solar wind propagation effects and limitations in the ionospheric model. There is also a large peak in the simulated power after 2230 UT that is absent in the observations. This discrepancy is puzzling because this peak is associated with a more strongly southward IMF at 2200 UT (at the WIND locations) which should increase the power.

Small scale oscillations in the solar wind dynamic pressure can again be seen. The solid black curves in both panels of Figure 6 show the power due parallel plasma flow. Again this power is only 0.1 to 0.3% of the total power deposited into the ionosphere. The dashed line in the first panel of Figure 6 shows the solar wind dynamic pressure shifted by 37 minutes to account for solar wind propagation from the WIND location; in the second panel the dashed line represent the IMF B_z component shifted by the same amount. It is interesting to note that each peak in the solar wind dynamic pressure again seems to correspond to a peak in the calculated power (Figure 4).

4. Summary

This study used observations and MHD modeling together to investigate the relationship between solar wind variations and energy deposited into the ionosphere during two substorm events. During periods of southward IMF the MHD simulation showed that an increase in the power deposited into the ionosphere. Large scale variations in the simulated power usually corresponded to those in the observations. These variations seem to be correlated with the IMF Bz component. The simulations also revealed short time scale oscillations that were driven by the dynamic pressure fluctuations. Despite the limitation of the MHD model, the simulation captured important features of the substorms.

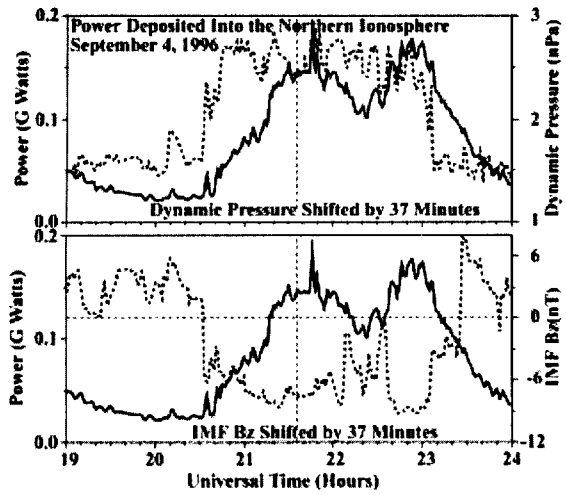

Figure 6. The black curves show the simulated power deposited into the northern hemisphere ionosphere due to the parallel plasma bulk flow.

Acknowledgments

This work was supported by grants from NASA NRA grant NAG5-9255 and by NASA grant ISTP NAG5-11704. Computing resources were provided by the National Resource Allocations Committee (NRAC), and the San Diego Supercomputing Center. UCLA-IGPP publication 5763.

References

Ashour-Abdalla, M., M. El-Alaoui, V. Peroomian, R. J. Walker, L.M. Zelenyi, L.A. Frank and W.R. Paterson, Localized reconnection and substorm onset on Dec. 22, 1996, *Geophys. Res. Lett., 26*, 3545, 1999.

Ashour-Abdalla, M., J. Raeder, M. El-Alaoui, and V. Peroomian, Magnetotail structure and its internal particle dynamics during northward IMF, in *New Perspective of the Earth's Magnetotail*, edited by A. Nishida, D.N. Baker and S.W.H. Cowley, *Geophys. Monogr., 105*, p. 77., AGU, Washington D.C, 1998.

Berchem, J., et al., The distant tail at 200 R_E: Comparisons between Geotail observations and the result of global MHD simulations, *J. Geophys. Res., 103*, 9121, 1998a.

El-Alaoui , M., Current disruption during November 24, 1996, substorm, *J. Geophys. Res., 106*, 6229, 2001.

Fedder, J.A., S.P. Slinker, J.G. Lyon, R.D. Elphinstone, Global numerical simulation of the growth phase and the expansion phase onset for a substorm observed by Viking, *J. Geophys. Res., 100*, 19083, 1995.

Frank, L. A., J. B. Sigwarth, W. R. Paterson, and S. Kokubun, Two encounters of the substorm onset region with Geotail spacecraft. *J. Geophys. Res., 106*, 5811, 1995

Frank, L. A., et al., Observations of plasmas and magnetic field in Earth's distant magnetotail: Comparison with a global MHD model, *J. Geophys. Res., 100*, 19,177, 1995.

Kennel, C. F., and H. E. Petschek, Limit on stably trapped particle fluxes, *J. Geophys. Res.*, 71, 1, 1966.

Knight, S., Parallel electric fields, *Planet. Space Sci., 21*, 741, 1973.

Leboeuf, J. N., T. Tajima, C. F. Kennel, and J. M. Dawson, Global simulation of the time-dependent magnetosphere, *Geophys. Res. Lett., 5*, 609, 1978.

Lyon, J. G., S. H. Brecht, J. A. Fedder, and P. J. Palmadesso, The effect on the Earth's magnetotail from a shock in the solar wind, *Geophys. Res. Lett.*, 7, 721, 1980.

Lyons, L. R., D. Evans, and R. Lundin, An observed relation between magnetic field aligned electric fields and downward electron energy fluxes in the vicinity of auroral forms, *J. Geophys. Res., 84*, 457, 1979.

Moen, J., and A. Brekke, The solar flux influence on quiet time conductances in the auroral ionosphere, *Geophys. Res. Lett., 20*, 971, 1993.

Ogino, T., and R. J. Walker, A magnetohydrodynamic simulation of the bifurcation of the tail lobes during intervals with a northward interplanetary magnetic field, *Geophys. Res. Lett., 11*, 1018, 1984.

Raeder, J., et al., Boundary layer formation in the magnetotail: Geotail observations and comparisons with a global MHD simulation, *Geophys. Res. Lett.*, 24, 951, 1997.

Raeder, J., J. Berchem, M. Ashour-Abdalla, The geospace environment modeling grand challenge: Results from a global geospace circulation model, *J. Geophys. Res., 103*, 14787, 1998.

Robinson, R. M., R. R. Vondrak, K. Miller, T. Dabbs, and D. Hardy, On calculating ionospheric conductances from the flux and energy of precipitating electrons, *J. Geophys. Res., 92*, 2565, 1987.

Spiro, R. W., P. H. Reiff, and L. J. Maher, Precipitating electron energy flux and auroral zone conductances-an empirical model, *J. Geophys. Res., 87*, 8215, 1982.